PROCEEDINGS of the
23rd International Congress on Acoustics

9 to 13 September 2019 in Aachen, Germany

Adaptation of the equivalent-fluid model to the additively manufactured acoustic porous materials

Kamil C. OPIELA(1), Tomasz G. ZIELIŃSKI(1)

(1)Institute of Fundamental Technological Research of the Polish Academy of Sciences, Poland, tzielins@ippt.pan.pl

ABSTRACT

Recent investigations show that the normal incidence sound absorption in 3D-printed rigid porous materials is eminently underestimated by numerical calculations using standard models. In this paper a universal amendment to the existing mathematical description of thermal dispersion and fluid flow inside rigid foams is proposed which takes account of the impact of the additive manufacturing technology on the acoustic properties of produced samples. The porous material with a motionless skeleton is conceptually substituted by an equivalent fluid with effective properties evaluated from the Johnson-Champoux-Allard-Pride-Lafarge model. The required macroscopic transport parameters are computed from the microstructural solutions using the hybrid approach. A cross-functional examination of the quality (shape consistency, representative surface roughness, etc.) of two periodic specimens obtained from additive manufacturing processes is additionally performed in order to link it to the results of the multiscale acoustic modelling. Based on this study, some of the transport parameters are changed depending on certain quantities reflecting the actual quality of a fabricated material. The developed correction has a considerable influence on the predicted value of the sound absorption coefficient such that the original discrepancies between experimental and numerical curves are significantly diminished.

Keywords: rigid porous material, additive manufacturing, sound absorption

1. INTRODUCTION

It is popularly known that porous materials are effective acoustic insulators. They possess superior damping properties due to a specific internal structure consisting of a solid skeleton and voids (pores) filled with fluid. By modifying the spatial distribution and geometry of voids, among others, one can directly influence the overall acoustic performance of a porous layer. Thus, knowing the correspondence between the design and the relevant characteristics of such media, it is possible to develop a particular configuration of a required behavior. Scientists have excogitated a multiscale theory to effectively predict the acoustic wave propagation and sound absorption in rigid porous materials using microstructure-based solutions for various cases, namely: for open-cell aluminium foams [13, 14], perforated closed-cell metallic foams [2], ceramic foams with spherical pores [17], polymeric foams [4, 5, 10, 11], double-porosity foams [3], syntactic hybrid foams (i.e., open-cell polyurethane foams with embedded hollow microbeads) [12], 3D-printed foams [18], granular [6, 7, 16] and fibrous media [8, 15, 19]. Nevertheless, many important issues still need to be investigated, especially vis-à-vis the usage of this approach to estimate the thermal and viscous effects connected with the wave propagation inside materials produced by popular, nowadays widely spread and continuously evolving additive manufacturing techniques. Since they are actually one of the few strategies that allow forming porous samples with a definite microstructure albeit not flawless, adopting appropriate model enhancements that will accomodate computations to reality should eventually lead to substantial benefits from practical point of view.

A sequence of calculations and measurements is performed to figure out the possibilities in estimating sound absorption of 3D-printed porous geometries with high precision. Two periodic samples are designed, fabricated, and investigated in terms of their quality and acoustic properties. The experimental and numerical normal incidence absorption curves are compared, and a study of the corresponding transport parameters is made for each geometry. The discussion is additionally based on the computed effective density and bulk modulus plots.

2. DESIGN AND MANUFACTURING OF PERIODIC POROUS MATERIALS

Prototyping of customised and complex three-dimensional geometries has recently become feasible with an additive manufacturing technique popularly known as 3D printing [9]. The strategy relies on the principle that the layers of material are successively formed on top of each other and fused together, eventually leading to the final object. The relevant production capabilities of such a method, however, depend to a large extent on its particular variant used. Manufacturing of sound-absorbing porous samples entails the necessity of using a high precision approach due to modest pore characteristic sizes. Most prevalent and relatively cheap machines operate based on the fused deposition modelling (FDM) printing technology [9]. In it a continuous filament made of a thermoplastic polymer is heated to the melting temperature at the nozzle, and extruded either onto the platform or on top of an already existing element. As a rather primitive method it often results in inconsistent dimensions and degenerate shapes with significant deviations (at least from the microscopic point of view) as well as other tough issues. Moreover, the achievable detail size usually do not exceed a few millimetres due to large layer thicknesses available.

The FDM printing technology was used to fabricate periodic porous samples in this research. Two fairly different but simple morphologies were proposed. The first one consists of a $10 \times 10 \times 12$ array of representative cubic cells (see Figure 1a) of side length equal 3 mm that contain only one central pore and six mutually perpendicular vertical as well as horizontal cylindrical channels (in Figures 1a and 1b the cell is shifted in the vertical direction by half of its characteristic size). In the following analysis they are therefore referred to as the One-Pore-Cells (OPC) with detailed dimensions listed in Table 1. In fact, the values shown there are not consistent with the designed, original values (for both geometries), but were decreased a bit (0.12 mm from each radius) in order to reflect the material shrinkage in 3D-printed objects.

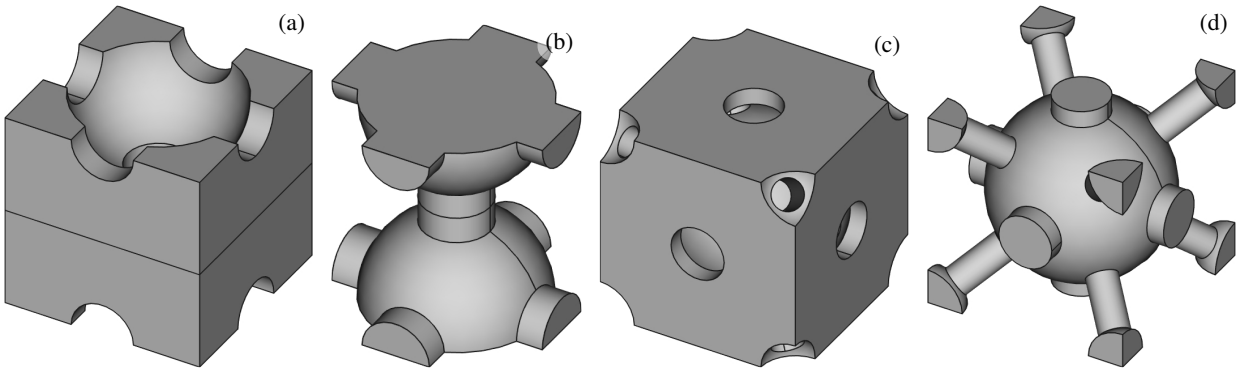

Figure 1. The designed Representative Unit Cells: (a) the OPC geometry; (b) the domain of fluid in the OPC geometry; (c) the NPC geometry; and (d) the domain of fluid in the NPC geometry.

Table 1. Diameters of pores and channels in the periodic cubic cells of size 3 mm (OPC) and 5 mm (NPC).

	Diameter [mm]			
Geometry	large pore	small pore	wide channel	narrow channel
OPC	2.46	–	0.96	–
NPC	4.36	1.76	1.36	0.76

The second devised representative element is more complicated. It is called the Nine-Pore-Cell (NPC) because it is comprised of nine spherical pores (or their parts) in total (one central, and eight one-eights of small corner ones) connected by cylindrical oblique narrow channels (see Figure 1c). It forms a $6 \times 6 \times 12$ array of 5 mm cubic cells that are additionally linked by wide channels in three directions. All the dimensions describing the geometry are given in Table 1. Both arrays of OPC and NPC cells were virtually cut such that to obtain a 36 and 60 mm-long cylinders, respectively, of diameter 29 mm that fit well to the impedance tube for acoustic material testing.

The manufactured porous specimens were examined in twofold way: the microgeometry of the produced sample was verified by the aid of a microscope, and the true porosity measurements were conducted on three different devices. As it was expected, the surface of the samples is quite rough and a little deformed (see, for example, the channel edges or 'wrinkles' in Figure 2), whereas the open porosity has greatly increased during the FDM process compared to its theoretical, numerically calculated value. It was evaluated as a consequence of force measurements and by weighting the samples on electronic scales of different quality after estimating

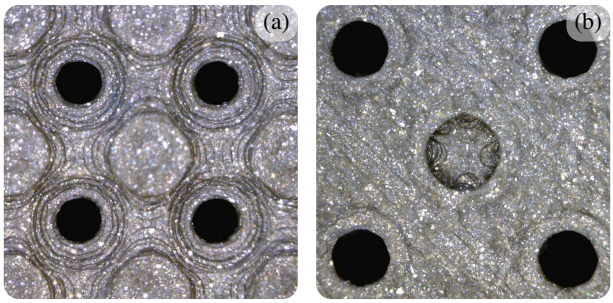

Figure 2. Microscopic verification of the quality of the fabricated samples: (a) top view (zoom) of the OPC sample; (b) top view (zoom) of the NPC sample.

the material mass density from six regularly-shaped objects of various sizes (the value agreed with its analogue given in product specifications), and the results are consistent, as shown in Table 2.

Table 2. Open porosity in computations and measurements: calculated numerically and measured by means of the gravity force as well as low (A) and high quality scales (B).

	Porosity, ϕ [–]			
Geometry	Calculated	Measured—force	Measured—mass A	Measured—mass B
OPC	0.3398	0.4488	0.4480	0.4493
NPC	0.4345	0.5394	0.5488	0.5513

3. MODELLING, EXPERIMENTS, AND INVERSE CHARACTERISATION

There exist three basic techniques based on the Finite Element Method for a numerical prediction of sound propagation and absorption in rigid porous media:

1. the Direct Simulation founded on solving a harmonic compressible viscous flow of fluid through the porous region (the Navier-Stokes equations);
2. the Direct Multiscale method in which viscous and thermal harmonic analyses are made for each frequency, f, on the representative volume of fluid in a periodic cell; and
3. the Hybrid Multiscale approach, where the region of fluid corresponding to a given unit periodic cell is fed to several geometrical and static finite element analyses of microstructural problems, the output of which then constitutes the basis for further considerations on macroscopic acoustic characteristics of this class of materials—the so called *transport parameters*.

In the latter case, one calculates the porosity, ϕ, and thermal characteristic length, Λ', directly from the porous morphology (e.g., the one shown in Figures 1b and 1d, as it was done in this work), from the character of an incompressible viscous flow (the Stokes problem) the static viscous permeability, k_0, and static thermal tortuosity, α_0, are deduced, the solution to the electric conduction problem (the Laplace equation) gives necessary information about the inertial tortuosity, α_∞, and viscous characteristic length, Λ, whereas static thermal permeability, k_0', and static thermal tortuosity, α_0', are found from the Poisson problem (thermal dispersion). The damping behaviour of the material backed by a rigid wall is then efficiently assessed by the properties of an equivalent fluid, that is the complex-valued dynamic effective mass density, $\rho_{\text{eff}}(f)$, and the dynamic effective bulk modulus, $K_{\text{eff}}(f)$, functions, according to the following formulae:

$$A(f) = 1 - |R(f)|^2, \qquad R(f) = \frac{Z(f) - Z_0}{Z(f) + Z_0} \tag{1}$$

and

$$Z(f) = -\mathrm{i}\sqrt{\rho_{\text{eff}}(f) K_{\text{eff}}(f)}\cot\left(\frac{2\pi f \ell \sqrt{\rho_{\text{eff}}(f)}}{\sqrt{K_{\text{eff}}(f)}}\right), \tag{2}$$

where $A(f)$ is the acoustic absorption coefficient, $R(f)$ is the reflection coefficient, $Z_0 = \rho_0 c_0$ is the characteristic impedance of the pore-fluid, ρ_0 and c_0 are the density and speed of sound in the pore-fluid, and, finally,

ℓ is the thickness of a porous medium. Knowing that

$$\rho_{\text{eff}}(f) = \frac{\rho_0\,\alpha(f)}{\phi} \qquad \text{and} \qquad K_{\text{eff}}(f) = \frac{K_0}{\phi\beta(f)} \qquad \text{with} \qquad \beta(f) = \gamma - \frac{\gamma-1}{\alpha'(f)}, \tag{3}$$

the surface acoustic impedance, $Z(f)$, can be equivalently expressed as:

$$Z(f) = -\frac{\mathrm{i}Z_0}{\phi}\sqrt{\frac{\alpha(f)}{\beta(f)}}\cot\left(\frac{2\pi f\ell}{c_0}\sqrt{\alpha(f)\beta(f)}\right). \tag{4}$$

Here $K_0 = \gamma p_0$ is the bulk modulus of the fluid in pores, γ is the heat capacity ratio of fluid in pores, p_0 denotes the ambient mean pressure, and $\alpha(f)$ as well as $\alpha'(f)$ stand for the dynamic (visco-inertial) tortuosity and the dynamic thermal tortuosity functions, respectively. Various models were developed and are utilised to approximate the dynamic tortuosity functions. Among them one finds the most advanced semi-phenomenological model by Johnson-Champoux-Allard-Pride-Lafarge (JCAPL) that requires all eight transport parameters and some crucial physical properties of the fluid in pores like the dynamic viscosity, μ, the Prandtl number, N_{Pr}, and the density, ρ_0. It looks as follows:

$$\alpha(f) = \alpha_\infty + \frac{\mu}{2\mathrm{i}\pi f\rho_0}\frac{\phi}{k_0}\left[\sqrt{\frac{2\mathrm{i}\pi f\rho_0}{\mu}\left(\frac{2\alpha_\infty k_0}{\Lambda\phi}\right)^2 + b^2} - b + 1\right], \qquad b = \frac{2{\alpha_\infty}^2 k_0}{\Lambda^2\phi(\alpha_0-\alpha_\infty)}, \tag{5}$$

$$\alpha'(f) = 1 + \frac{\mu}{2\mathrm{i}\pi f\rho_0 N_{\text{Pr}}}\frac{\phi}{k_0'}\left[\sqrt{\frac{2\mathrm{i}\pi f\rho_0 N_{\text{Pr}}}{\mu}\left(\frac{2k_0'}{\Lambda'\phi}\right)^2 + b'^2} - b' + 1\right], \qquad b' = \frac{2k_0'}{\Lambda'^2\phi(\alpha_0'-1)}. \tag{6}$$

In this work, this particular model was incorporated for the purposes of the evaluation of the effective dynamic functions $\rho_{\text{eff}}(f)$ and $K_{\text{eff}}(f)$ needed to compute the coefficient, $A(f)$.

The overall sound absorption properties of the analysed specimens were determined from experiments carried out in the 29 mm impedance tube following the procedure described in the ISO 10534-2 Standard [1] published in 1998. Furthermore, the acoustic transport parameters were found from the respective 3D problems of the Hybrid Multiscale method. Figures 3 and 4 present the convergence of these parameters with respect to the Finite Element meshes generated on the representative fluid regions (see Figures 1b and 1d once again) for the One-Pore-Cell and Nine-Pore-Cell geometries, respectively. The final, reference computations shown later on in this section were done on the finest grids, where the values of transport parameters are nearly converged.

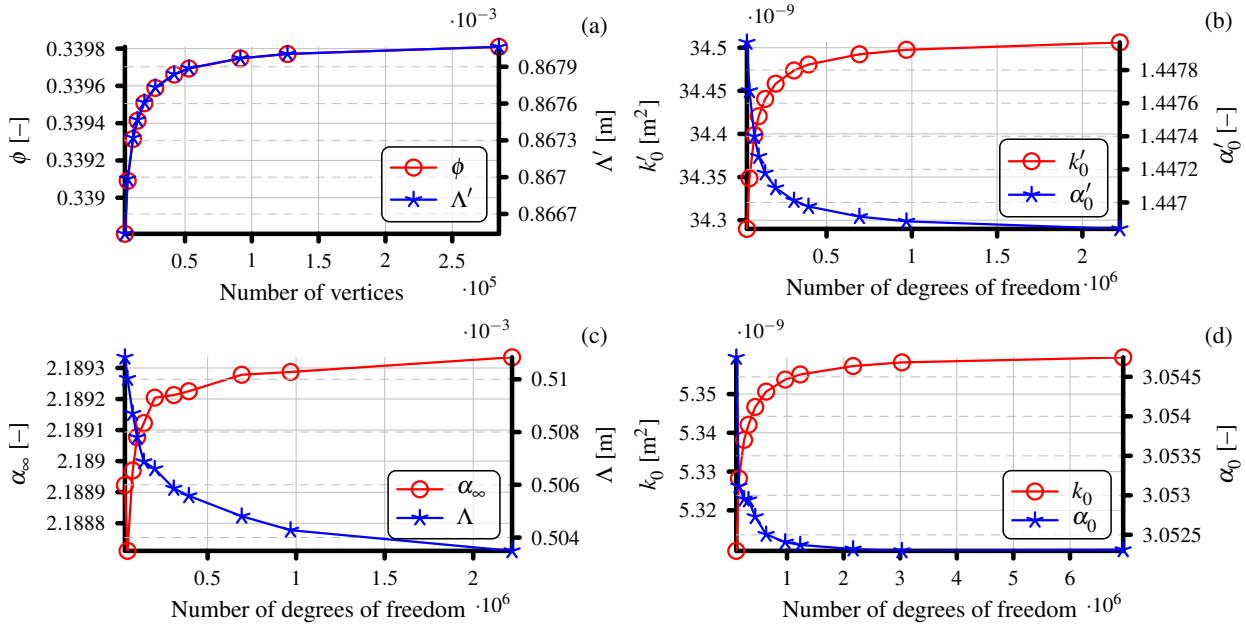

Figure 3. Mesh convergence with respect to the computed transport parameter values of the OPC domain: (a) the geometrical analysis, (b) the Poisson problem, (c) the Laplace problem, and (d) the Stokes problem.

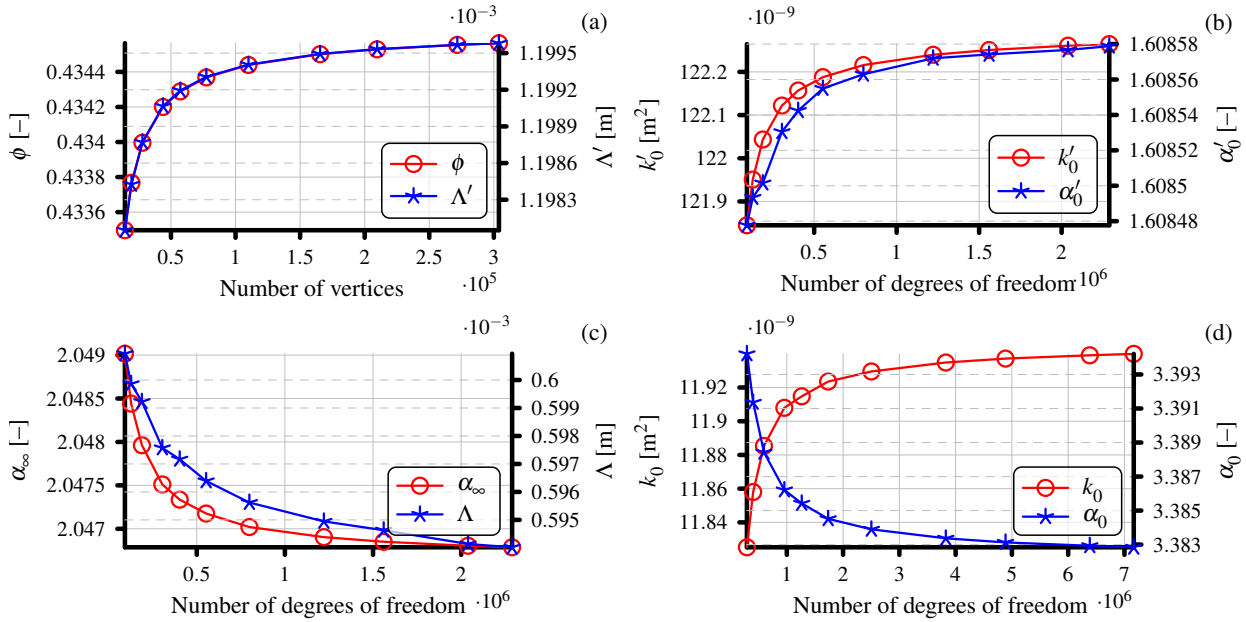

Figure 4. Mesh convergence with respect to the computed transport parameter values of the NPC domain: (a) the geometrical analysis, (b) the Poisson problem, (c) the Laplace problem, and (d) the Stokes problem.

It has been already shown that the wave attenuation effects in fabricated rigid-porous layers are eminently underestimated by numerical calculations using standard models (see, e.g., [18]). The obtained results do confirm this observation. Table 3 collects the determined values of transport parameters for the OPC and NPC samples leading to the curves shown in Figures 5–7. A large discrepancies between computed and experimental plots of $\rho_{\text{eff}}(f)/\rho_0$, $K_{\text{eff}}(f)/K_0$ and $A(f)$ are clearly visible. In order to get to know right values, an inverse characterisation procedure was undertaken. It was based on the least squares problem arising from the minimisation of the difference between the measurements of sound absorption and their analytically constructed counterparts. Indeed, the achieved agreement between the respective curves is very good (see Figures 6 and 7). The credibility of the gathered results (see Table 3) is gained by realising the fact, that the values of the identified porosities in both cases (OPC and NPC) are very close to the measured ones (cf. Table 2). Moreover, its high level is sustained by performing the following consideration. Surface acoustic impedance is a periodic complex function with a period of π. Therefore, there exists a similarity number, n, for which it takes exactly the same value for a given argument f (cf. (4)):

$$\cot\left(\frac{2\pi f\ell}{c_0}\sqrt{\alpha(f)\beta(f)}\right) = \cot\left(\frac{2\pi f\ell}{c_0}\sqrt{\alpha(f)\beta(f)}+n\pi\right) = \cot\left(\frac{2\pi f\ell}{c_0}|\hat{n}|\sqrt{\alpha(f)\beta(f)}\right), \quad n\in\mathbb{Z}. \tag{7}$$

Hence, the similarity number $\hat{n}$ that scales both $\alpha(f)$ and $\beta(f)$ such that $Z(f)$ remains unchanged can be evaluated as:

$$\hat{n} = 1 + \frac{nc_0}{2f\ell\sqrt{\alpha(f)\beta(f)}}. \tag{8}$$

We denote the family of density and bulk modulus effective functions yielding identical values for different

Table 3. Computed and identified transport parameters. For each geometry the relative change of the computed values during the identification procedure is also presented.

	Transport parameters							
Geometry, case	ϕ [–]	k_0 [10^{-9} m^2]	k_0' [10^{-9} m^2]	α_∞ [–]	α_0 [–]	α_0' [–]	Λ [mm]	Λ' [mm]
OPC, computed	0.3398	5.359	34.51	2.189	3.052	1.447	0.5035	0.8681
OPC, identified	0.4546	2.824	21.74	2.155	2.707	1.410	0.3245	1.294
OPC, relative	1.3379	0.5269	0.6301	0.9844	0.8869	0.9742	0.6445	1.4905
NPC, computed	0.4345	11.94	122.3	2.047	3.383	1.609	0.5940	1.200
NPC, identified	0.5567	17.42	140.7	1.923	3.301	1.697	0.3605	0.8386
NPC, relative	1.2811	1.4589	1.1505	0.9395	0.9758	1.0551	0.6068	0.6991

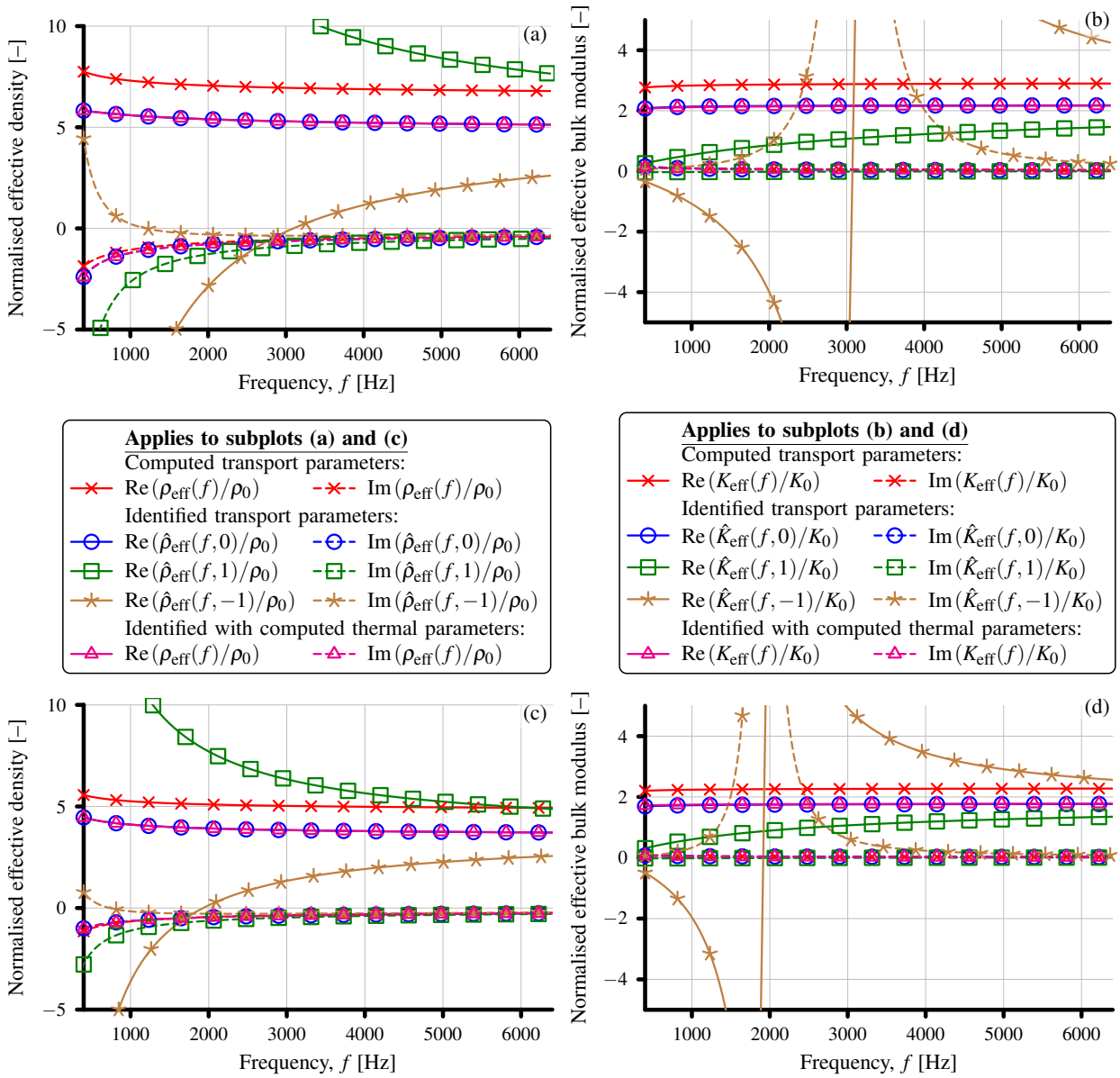

Figure 5. Normalised effective mass density (a,c) and bulk modulus (b,d) of a porous layer made of either the OPC (a,b) or NPC (c,d) geometries.

factors n as

$$\hat{\rho}_{\mathrm{eff}}(f,n) = \frac{\rho_0 \hat{n} \alpha(f)}{\phi} \qquad \text{and} \qquad \hat{K}_{\mathrm{eff}}(f,n) = \frac{K_0}{\hat{n}\phi\beta(f)}\,. \tag{9}$$

Plotting the functions $\hat{\rho}_{\mathrm{eff}}(f,n)/\rho_0$ as well as $\hat{K}_{\mathrm{eff}}(f,n)/K_0$ for $n \in \{-1,0,1\}$ corresponding to the identified transport parameters and comparing them with the calculated $\rho_{\mathrm{eff}}(f)/\rho_0$ and $K_{\mathrm{eff}}(f)/K_0$ by means of the Hybrid Multiscale method reveals the efficacy of the adopted inverse characterisation algorithm—the results for $n = 0$ are closer to the reference, 'ideal' curves ($\rho_{\mathrm{eff}}(f)/\rho_0$ and $K_{\mathrm{eff}}(f)/K_0$ with computed transport parameters) than those pertaining to $n = 1$ and $n = -1$.

After obtaining the identified transport parameters, a simple sensitivity analysis was performed by modifying only particular computed values in accordance with the identification procedure and plotting the resulting absorption curves. It was found out that the change of the three thermal transport parameters, namely the static thermal permeability, k_0', static thermal tortuosity, α_0', and thermal characteristic length, Λ', does not have much impact on the related sound absorption, albeit the relative decrease or increase of k_0' and Λ' during the identification procedure was considerable for both geometries (see the relative values in Table 3). The plots drawn using the full set of eight identified parameters are virtually the same as those curves proceeded from five identified and three computed parameters, being the thermal ones (Figures 6 and 7).

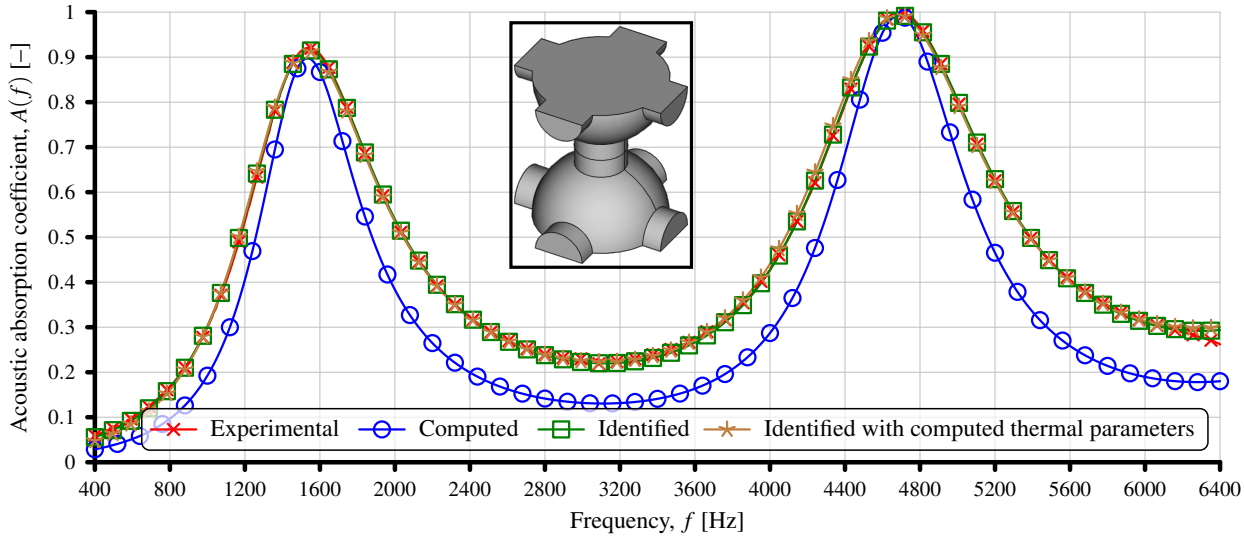

Figure 6. Normal incidence sound absorption of a rigidly backed 35.72 mm-thick porous layer made of the OPC geometry.

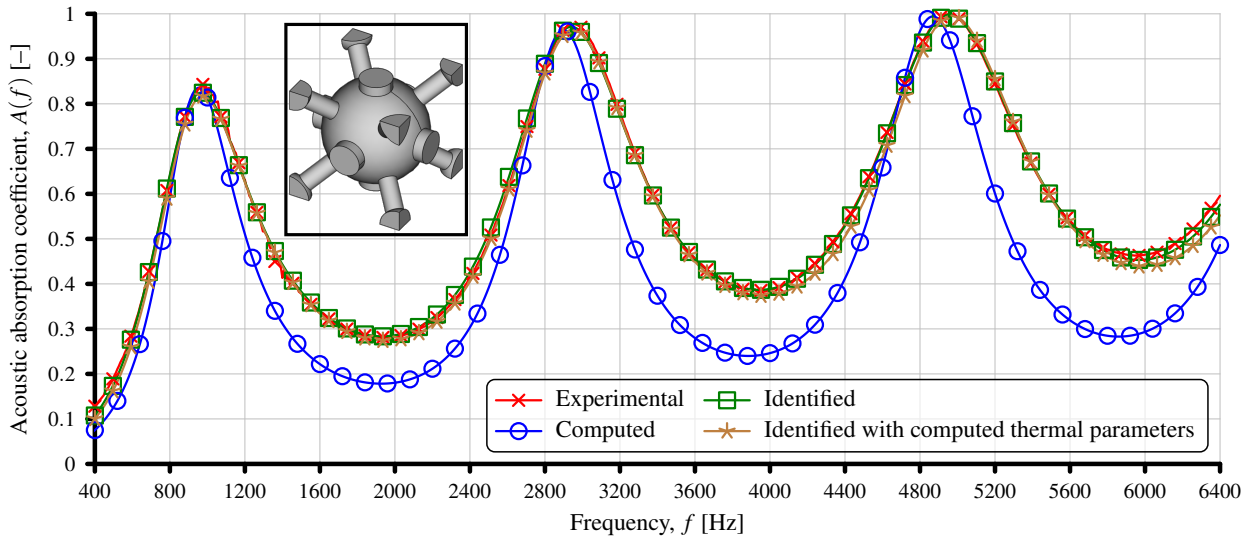

Figure 7. Normal incidence sound absorption of a rigidly backed 59.7 mm-thick layer made of the NPC cells.

4. CONCLUSIONS

It is rather understandable that the fabricated objects can mirror the designed ideal geometry of representative cells to just a certain degree, depending on the resolution and precision of a given technology. It is believed, that the inconsistency between experimental and simulation results is due to various reasons, including surface defects, material shrinkage, and bounded accuracy. At the current stage of research it has been found that porous materials 3D-printed in the FDM technology have much higher porosity and are characterised by different visco-inertial transport parameters than those calculated from the microstructural analyses. The thermal transport parameters, on the other hand, that is the static thermal permeability, k_0', static thermal tortuosity, α_0', and thermal characteristic length, Λ', seem to remain unchanged during the manufacturing process. This knowledge may open new possibilities in the (still ongoing) development of the universal amendment to the existing mathematical models describing thermal dispersion and fluid flow inside 3D-printed rigid foams.

ACKNOWLEDGEMENTS

The financial support of Project No. 2015/19/B/ST8/03979: “Relations between the micro-geometry and sound propagation and absorption in porous and poroelastic media”, financed by the Polish National Science Centre (NCN), is gratefully acknowledged.

REFERENCES

[1] ISO 10534-2: Determination of sound absorption coefficient and impedance in impedance tubes, 1998.

[2] Chevillotte, F.; Perrot, C.; Panneton, R. Microstructure based model for sound absorption predictions of perforated closed-cell metallic foams. J. Acoust. Soc. Am., 128(4), 2010, 1766–1776.

[3] Chevillotte, F.; Perrot, C.; Guillon, E. A direct link between microstructure and acoustical macro-behavior of real double porosity foams. J. Acoust. Soc. Am., 134(6), 2013, 4681–4690.

[4] Doutres, O.; Ouisse, M.; Atalla, N.; Ichchou, M. Impact of the irregular microgeometry of polyurethane foam on the macroscopic acoustic behavior predicted by a unit-cell model. J. Acoust. Soc. Am., 136(4), 2014, 1666–1681.

[5] Gao, K.; van Dommelen, J. A. W.; Geers, M. G. D. Investigation of the effects of the microstructure on the sound absorption performance of polymer foams using a computational homogenization approach. European Journal of Mechanics. A/Solids, 61, 2017, 330–344.

[6] Gasser, S.; Paun, F.; Bréchet, Y. Absorptive properties of rigid porous media: Application to face centered cubic sphere packing. J. Acoust. Soc. Am., 117(4), 2005, 2090–2099.

[7] Lee, C.-Y.; Leamy, M. J.; Nadler, J. H. Acoustic absorption calculation in irreducible porous media: A unified computational approach. J. Acoust. Soc. Am., 126(4), 2009, 1862–1870.

[8] Luu, H. T.; Perrot, C.; Panneton, R. Influence of porosity, fiber radius, and fiber orientation on anisotropic transport properties of random fiber structures. J. Acoust. Soc. Am., 141(5), 2017, 3888.

[9] Ngo, T. D.; Kashani, A.; Imbalzano, G.; Nguyen, K. T. Q.; Hui, D. Additive manufacturing (3D printing): A review of materials, methods, applications and challenges. Composites Part B: Engineering, 143, 2018, 172–196.

[10] Park, J. H.; Minn, K. S.; Lee, H. R.; Yang, S. H.; Yu, C. B.; Pak, S. Y.; Oh, C. S.; Song, Y. S.; Kang, Y. J.; Youn, J. R. Cell openness manipulation of low density polyurethane foam for efficient sound absorption. J. Sound Vib., 406, 2017, 224–236.

[11] Park, J. H.; Yang, S. H.; Lee, H. R.; Yu, C. B.; Pak, S. Y.; Oh, C. S.; Kang, Y. J.; Youn, J. R. Optimization of low frequency sound absorption by cell size control and multiscale poroacoustics modeling. J. Sound Vib., 397, 2017, 17–30.

[12] Park, J. H.; Yang, S. H.; Minn, K. S.; Yu, C. B.; Pak, S. Y.; Song, Y. S.; Youn, J. R. Design and numerical analysis of syntactic hybrid foam for superior sound absorption. Materials & Design, 142, 2018, 212–220.

[13] Perrot, C.; Panneton, R.; Olny, X. Periodic unit cell reconstruction of porous media: Application to open-cell aluminum foams. J. Appl. Phys., 101:113538 (1–11), 2007.

[14] Perrot, C.; Chevillotte, F.; Panneton, R. Dynamic viscous permeability of an open-cell aluminum foam: Computations versus experiments. J. Appl. Phys., 103:024909 (1–8), 2008.

[15] Ren, S.; Ao, Q.; Meng, H.; Xin, F.; Huang, L.; Zhang, C.; Lu, T. J. A semi-analytical model for sound propagation in sintered fiber metals. Composites Part B: Engineering, 126, 2017, 17–26.

[16] Zieliński, T. G. Microstructure-based calculations and experimental results for sound absorbing porous layers of randomly packed rigid spherical beads. J. Appl. Phys., 116(3):034905 (1–17), 2014.

[17] Zieliński, T. G. Generation of random microstructures and prediction of sound velocity and absorption for open foams with spherical pores. J. Acoust. Soc. Am., 137(4), 2015, 1790–1801.

[18] Zieliński, T. G. Pore-size effects in sound absorbing foams with periodic microstructure: modelling and experimental verification using 3D printed specimens. In: Sas, P.; Moens, D.; van de Walle, A. (editors). Proceedings of ISMA2016 International Conference on Noise and Vibration Engineering/USD2016 International Conference on Uncertainty in Structural Dynamics, Heverlee, Belgium, September 2016, 95–104.

[19] Zieliński, T. G. Microstructure representations for sound absorbing fibrous media: 3D and 2D multiscale modelling and experiments. J. Sound Vib., 409(6), 2017, 112–130.